A heat-transfer and fluid-flow-based model to obtain a specific weld geometry using various combinations of welding variables

S. Mishra and T. DebRoy[a)]

Department of Materials Science and Engineering, The Pennsylvania State University,
University Park, Pennsylvania 16802

Numerical heat transfer and fluid flow models have provided significant insight into welding processes and welded materials that could not have been achieved otherwise. However, the use of these models has been limited by two major problems. First, the model predictions do not always agree with the experimental results because some input parameters such as the arc efficiency cannot be accurately prescribed. Second, and more important, these models cannot determine multiple pathways or sets of welding variables that can lead to a particular weld attribute such as the weld pool geometry, which is defined by an equilibrium temperature surface. Here we show that the computational heat transfer and fluid flow models of fusion welding can overcome the aforementioned difficulties by combining with a genetic algorithm. The reliability of the convective heat transfer model can be significantly improved by optimizing the values of the uncertain input parameters from a limited volume of the experimental data. Furthermore, the procedure can calculate multiple sets of welding variables, each leading to the same weld geometry. These multiple paths were obtained via a global search using a genetic algorithm within the phenomenological framework of the equations of conservation of mass, momentum, and energy. This computational procedure was applied to the gas tungsten arc welding of Ti–6Al–4V alloy to calculate various sets of welding variables to achieve a specified weld geometry. The calculated sets of welding parameters showed wide variations of values. However, each set of welding parameters resulted in a specified geometry showing the effectiveness of the computational procedure. © *2005 American Institute of Physics.* [DOI: 10.1063/1.2001153]

I. INTRODUCTION

In recent decades, the application of numerical transport phenomena has provided useful information about the thermal cycles and weld pool geometry in both linear and spot welding.[1–19] Computed temperatures have been used to quantitatively understand the evolution of phase composition,[15,20] grain structure,[6,7] inclusion structure,[16,21,22] and weld metal composition change owing to both the evaporation of alloying elements and the dissolution of gases.[8,13] Capabilities to quantitatively understand geometry, composition, and structure of welds in simple systems provide hope that one day welding engineers may be able to use numerical models to tailor weldment characteristics according to specifications.

Currently the numerical heat transfer and fluid flow codes for fusion welding are used mostly as a research tool rather than as a tool for designing and manufacturing in industry. There are several reasons for the restricted use of these advanced tools. First, the temperature fields and thermal cycles predicted by the numerical heat transfer and fluid flow models do not always agree with the experimental results. Second, the GTA welding system is highly complex and involves the nonlinear interaction of several welding variables. As a result, a particular weld attribute, such as the weld geometry, can be obtained through the use of various sets of welding variables. The current generation of numerical heat transfer and fluid flow models cannot determine alternative pathways to achieve a target weld attribute.

A primary reason for the disagreement between the computed and experimentally determined temperature fields is the uncertainty of the values of some of the input parameters because they cannot be prescribed based on either scientific principles or welding conditions. The models for the gas tungsten arc (GTA) welding process have five uncertain input parameters, i.e., arc efficiency, arc radius, power distribution factor, and the effective thermal conductivity and viscosity of the liquid metal. Although the values of arc efficiency have been experimentally measured for many welding conditions, the reported values vary significantly, even for apparently similar welding conditions. Measured values of the arc radius and power distribution factor depend on welding conditions and, as a result, their values cannot be accurately specified except for certain narrow windows of welding conditions. Values of the effective thermal conductivity and viscosity are important, since they allow accurate modeling of the high rates of transport of heat and mass in systems with strong fluctuating velocities, such as small weld pools with very strong convection currents. The values of effective conductivity and viscosity are properties of the specific welding system, and not the inherent physical properties of the liquid metal,[13,23] and the values of these parameters significantly affect the results of numerical heat transfer and fluid flow calculations. A systematic global search for the uncertain input parameters is needed so that the computed

---

[a)]Electronic mail: debroy@psu.edu

temperature profiles always agree with the corresponding experimentally determined values. The desired depth and width of the weld pool and the cooling rate are often specified to achieve a structurally sound and reliable welded joint. Therefore, an important requirement is to determine the values of the welding variables necessary for achieving a given weld attribute, such as the weld geometry. In practice a particular weld attribute may be obtained through multiple combinations of welding variables. The forward numerical model for the calculation of temperature and velocity fields needs to be systematically interrogated to estimate the optimized values of welding variable sets that can produce a specified weld geometry.

The aforementioned shortcomings of the conventional numerical heat transfer and fluid flow models can be overcome by the computational procedure described here. The procedure has been applied to the GTA welding of Ti–6Al–4V alloy, which is an important structural alloy of titanium. First, the reliability of the convective heat transfer model for GTA welding is improved by estimating the values of arc efficiency, arc radius, arc power distribution factor, and effective thermal conductivity and viscosity. The values of these five uncertain input parameters are estimated by using a real-number-based genetic algorithm (GA) and a limited volume of experimental data. The ability of the GA to find the global optimal solution independent of the initial guessed values[20,24,25] makes it appropriate for estimating these uncertain parameters. A comparison of the calculated and experimental geometries is undertaken to examine the reliability of the computational procedure. Next, the GA systematically searches for multiple sets of welding variables of arc current, voltage, and welding speed to obtain a specified weld geometry. Since the search involves the reliable numerical heat transfer and fluid flow forward model, the estimated sets of welding variables comply with the phenomenological laws of welding physics and improve with iterations following certain rules of evolution.[24–27] Thus, the proposed computational approach enables the calculation of multiple pathways or multiple sets of welding variables, each of which leads to the target weld geometry.

II. THE MATHEMATICAL MODEL

A. Modeling of heat transfer and fluid flow during gas tungsten arc welding

An incompressible, laminar and Newtonian liquid flow is assumed in the weld pool. The linear momentum conservation equation for the jth direction is given by[12,17,19]

$$\rho \frac{\partial u_j}{\partial t} + \rho \frac{\partial (u_i u_j)}{\partial x_i} = \frac{\partial}{\partial x_i}\left(\mu \frac{\partial u_j}{\partial x_i}\right) + S_j, \qquad (1)$$

where ρ is the density, t is the time, x_i is the distance along the $i=1$, 2, and 3 directions, u_j is the velocity component along the j direction, μ is the effective viscosity, and S_j is the source term for the jth momentum equation and is given as[12,17]

$$S_j = -\frac{\partial p}{\partial x_j} + \frac{\partial}{\partial x_j}\left(\mu \frac{\partial u_j}{\partial x_j}\right) - C\left(\frac{(1-f_L)^2}{f_L^3 + B}\right)u_j$$
$$- \rho U \frac{\partial u_i}{\partial x_i} + Sb_j, \qquad (2)$$

where p is the pressure, f_L is the liquid fraction, B is a constant introduced to avoid division by zero, $C(=1.6 \times 10^4)$ is a constant that takes into account mushy zone morphology, U is the welding speed, and Sb_j represents both the electromagnetic and buoyancy source terms. The third term on the right-hand side of Eq. (2) represents the frictional dissipation in the mushy zone according to the Carman-Kozeny equation for flow through a porous media.[28,29] It is assumed that the electromagnetic properties of the workpiece are temperature independent, so that the electrical conductivity and the magnetic permeability remain constant, and the problem is axisymmetric. The adequacy of this assumption has been discussed by Kou and Sun.[30]

The value of the effective viscosity in Eq. (1) is a property of the specific welding system, and not an inherent property of the liquid metal. Typical values of effective viscosity are much higher than that of the molecular viscosity.[31,32] The higher value is important because it allows accurate modeling of the high rates of transport of momentum in systems with strong fluctuating velocities that are inevitable in small weld pools with very strong convection currents.[32] Spatially independent values of effective viscosity and effective thermal conductivity are used in the calculations reported in this paper. An alternative approach would have been to use a turbulence model such as the commonly used K-ε model[33] to calculate the spatial distribution of viscosity in the weld pool. However, the K-ε model is computationally intensive and contains five empirical constants that have been determined for parabolic flows in large-scale systems. The validity of these five empirical constants in fairly small-scale weld pools with strong elliptic (recirculating) flows has never been rigorously tested. Thus, the adaptation of the K-ε model for the problem reported in this paper can only result in increased computational volume without any added assurance of the quality of the computed results. As a result, a computationally efficient, spatially independent, enhanced effective viscosity and enhanced thermal conductivity approach has been adopted here, and the effectiveness of the approach is examined by comparing the calculated weld pool geometry with the corresponding experimental results. The pressure field was obtained by solving the following continuity equation simultaneously with the momentum equation:[12,17]

$$\frac{\partial (pu_i)}{\partial x_i} = 0. \qquad (3)$$

The total enthalpy H is represented by a sum of sensible heat h and latent heat content ΔH, i.e., $H=h+\Delta H$, where $h = \int C_p dT$, C_p is the specific heat, T is the temperature, $\Delta H = f_L L$, L is the latent heat of fusion, and the liquid fraction f_L is assumed to vary linearly with temperature in the mushy zone:[12,17]

$$
f_L = \begin{cases} 1, & T > T_L, \\ \dfrac{T - T_S}{T_L - T_S}, & T_S \leqslant T \leqslant T_L, \\ 0, & T < T_S, \end{cases} \tag{4}
$$

where T_L and T_S are the liquidus and the solidus temperatures, respectively. The thermal energy transport in the weld workpiece can be expressed by the following modified energy equation:[12,17]

$$
\rho \frac{\partial h}{\partial t} + \rho \frac{\partial (u_i h)}{\partial x_i} = \frac{\partial}{\partial x_i}\left(\frac{k}{C_p}\frac{\partial h}{\partial x_i}\right) - \rho \frac{\partial \Delta H}{\partial t} - \rho \frac{\partial (u_i \Delta H)}{\partial x_i}
$$
$$
- \rho U \frac{\partial h}{\partial x_i} - \rho U \frac{\partial \Delta H}{\partial x_i}, \tag{5}
$$

where k is the effective thermal conductivity. In the liquid region, the value of the thermal conductivity in Eq. (5) is taken as the effective thermal conductivity, which is a property of the specific welding system and not an inherent property of the liquid metal. Typical values of the effective thermal conductivity are much higher than that of the thermal conductivity of the liquid. The higher value is important because it allows accurate modeling of the high rates of transport of heat in systems with strong fluctuating velocities that are inevitable in small weld pools with very strong convection currents.[29] Since the weld is symmetrical about the weld center line, only half of the workpiece is considered. The weld top surface is assumed to be flat. The velocity boundary condition is given by[12,17]

$$
\mu \frac{\partial u}{\partial z} = f_L \frac{d\gamma}{dT}\frac{\partial T}{\partial x},
$$

$$
\mu \frac{\partial v}{\partial z} = f_L \frac{d\gamma}{dT}\frac{\partial T}{\partial y},
$$

$$
w = 0, \tag{6}
$$

where $u, v,$ and w are the velocity components along the $x, y,$ and z directions, respectively, and $d\gamma/dT$ is the temperature coefficient of surface tension. As shown in Eq. (6), the u and v velocities at the surface are determined from the Marangoni effect.[12] The w velocity is zero since there is no flow of liquid metal perpendicular to the pool top surface. The heat flux at the top surface is given by[12,17]

$$
k \frac{\partial T}{\partial z} = \frac{dQ\eta}{\pi r_b^2}\exp\left(-\frac{d(x^2 + y^2)}{r_b^2}\right)
$$
$$
- \sigma\varepsilon(T^4 - T_a^4) - h_c(T - T_a), \tag{7}
$$

where r_b is the arc radius of a circular region within which the arc power is focused, d is the dimensionless arc power distribution factor, which determines the nature of distribution of the power density of the arc, Q is the total arc power, η is the arc efficiency, σ is the Stefan-Boltzmann constant, h_c is the heat transfer coefficient, and T_a is the ambient temperature. The first term on the right-hand side of Eq. (7) is the heat input from the heat source, defined by a Gaussian heat distribution. The arc power distribution factor d deter-

TABLE I. Welding variables and experimentally measuted weld pool penetration and width (Ref. 7).

Data set	Voltage (V)	Current (A)	Welding speed (mm/s)	Weld pool penetration (mm)	Weld pool width (mm)
1	19.5	111.0	0.5	2.7	20.2
2	19.2	111.0	1.0	2.0	12.6
3	19.8	111.0	2.0	1.5	12.0
4	19.8	111.0	4.0	1.1	9.6

mines the nature of the Gaussian heat distribution pattern. The distribution is rather diffused for low values of d such as 0.5 and more focused for higher values of d such as 3.0. The second and third terms represent the heat loss by radiation and convection, respectively. The boundary conditions are defined as zero flux across the symmetric surface (i.e., at $y = 0$) by[12,17]

$$
\frac{\partial u}{\partial y} = 0, \quad v = 0, \quad \frac{\partial w}{\partial y} = 0, \tag{8}
$$

and

$$
\frac{\partial h}{\partial y} = 0. \tag{9}
$$

At all other surfaces, the temperatures are taken as ambient temperature and the velocities are set to zero.

B. Genetic algorithm as an optimization model

A real-number-based genetic algorithm (GA) is first used to enhance the reliability of the numerical heat transfer and fluid flow model by estimating an optimum set of uncertain input parameters for the model, i.e., arc efficiency (η), arc radius (r_b), arc power distribution factor (d), effective thermal conductivity (k_{eff}), and effective viscosity (μ_{eff}). To start with, many initial sets of randomly chosen values of these unknown input parameters are created. A systematic global search is next undertaken to find the most optimum set of values of these unknown input parameters that leads to the least error between the calculated and the experimental weld pool dimensions, i.e., weld pool penetration and width. The experimental data consist of sets of four welding conditions and the corresponding measured weld pool dimensions, as given in Table I. The calculated weld pool penetration and width for each set of input welding variables are obtained from the numerical heat transfer and fluid flow model. The randomly chosen values of unknown input parameters do not always produce the desired weld dimensions. The resulting mismatch between the computed and the desired weld dimensions is expressed by the following objective function, O1(f):

$$
O1(f) = \sum_{m=1}^{4}\left[\left(\frac{p_m^c}{p_m^e} - 1\right)^2 + \left(\frac{w_m^c}{w_m^e} - 1\right)^2\right], \tag{10}
$$

where m is the index that identifies the specific set of welding conditions given in Table I, p_m^c and w_m^c are the computed

TABLE II. Data used in the calculations (see Ref. 7 and 15).

Physical property	Value
Liquidus temperature, T_1 (K)	1928.0
Solidus temperature, T_s (K)	1878.0
Density of metal, ρ(kg/m^3)	4000.0
Thermal conductivity of solid, k_s(J/m s K)	20.0
Specific heat of solid, C_{ps}(J/kg K)	610.0
Specific heat of liquid, C_{pl}, (J/kg K)	700.0
Temperature coefficient of surface tension, $d\gamma/dT$(N/m K)	-0.28×10^{-3}
Coefficient of thermal expansion, β(K^{-1})	1.1×10^{-5}
Viscosity of molten titanium, μ_{fl}(kg/m s)	4.9×10^{-3}
Composition of the electrode	W–2% Th
Electrode taper angle	60°
Radius of the electrode, e_r (mm)	1.0

weld pool penetration and width, respectively, and p_m^e and w_m^e are the corresponding experimental or desired values of these two weld attributes for the set of welding conditions with index m. The objective function O1(f) depends on the five unknown input parameters:

$$O1(f) = O1(f_1, f_2, f_3, f_4, f_5) = O1\left(\eta, \frac{r_b}{e_r}, d, \frac{k_{\text{eff}}}{k_s}, \frac{\mu_{\text{eff}}}{\mu_{\text{fl}}}\right). \quad (11)$$

In Eq. (11), e_r is the radius of the electrode, k_s is the thermal conductivity of the solid metal at room temperature, μ_{fl} is the viscosity of molten titanium, k_{eff} is the effective thermal conductivity of the liquid metal, and μ_{eff} is the effective viscosity of the liquid metal. These are reference values that represent the order of magnitude of the unknown input parameters. These reference values and other data needed for the calculations are given in Table II. Note that Eq. (11) has been made nondimensional in order to preserve the importance of all five unknown input parameters, making their nondimensional values comparable in magnitude. The GA produces new individuals, or sets of unknown input parameters, with iterations based on the evolutionary principles.[20,26,27] The GA used in the present study is a parent centric recombination (PCX) operator-based generalized generation gap (G3) model.[20,26,27] The specific application of this model for obtaining the optimum set of values of the five unknown input parameters of the heat transfer and fluid flow model for GTA welding is described in the Appendix.

Once an optimum set of values of the five unknown input parameters enhances the reliability of the calculated results, the GA is used to search for multiple sets of important welding variables, i.e., arc current, voltage, and welding speed to achieve a target weld geometry. The search starts by creating many initial sets of randomly chosen values of the three welding variables. This is followed by a global search for multiple sets of values of these three variables, leading to the least error between the calculated and the target weld pool dimensions, i.e., penetration and width. The heat transfer and fluid flow model calculates the values of these weld dimensions for each set of input welding variables. The chosen values of welding variables do not always produce the

desired weld dimensions, and the resulting mismatch between the computed and the desired weld dimensions is expressed by the following objective function, O2(f):

$$O2(f) = \left(\frac{p^c}{p^e} - 1\right)^2 + \left(\frac{w^c}{w^e} - 1\right)^2, \quad (12)$$

where p^c and w^c are the computed weld pool penetration and width, respectively, and p^e and w^e are the corresponding experimental values of these two weld attributes for the target weld geometry chosen for the study. The objective function O2(f) depends on the three welding variables: current I, voltage V, and welding speed U.

$$O2(f) = O2(f_1, f_2, f_3) = O2\left(\frac{I}{I_r}, \frac{V}{V_r}, \frac{U}{U_r}\right), \quad (13)$$

where I_r, V_r, and U_r are the reference values that represent the order of magnitude of the welding variables. Note that Eq. (13) has been made nondimensional in order to preserve the importance of all three welding variables by making their nondimensional values comparable in magnitude. Again, the GA produces new individuals, or sets of welding conditions, with iterations based on the evolutionary principles.[20,26,27] The specific application of this model for obtaining the multiple sets of welding variables to achieve a target weld geometry is the same as that described in Appendix; however, an individual in a population of GA now consists of a set of values of the three welding variables, instead of a set of values of the five unknown input parameters.

III. RESULTS AND DISCUSSION

A. Improving the reliability of the heat transfer and fluid flow calculations

Since the calculations of temperature and velocity fields are based on well-established principles of heat transfer and fluid flow, the lack of reliability of the computed results originate from the uncertain values of the input parameters that cannot be specified from welding conditions. In order to address this problem, values of arc efficiency (η), arc radius (r_b), arc power distribution factor (d), effective thermal conductivity of the molten metal (k_{eff}), and effective viscosity of the molten metal (μ_{eff}) were determined from a limited volume of experimental data using a genetic-algorithm-based global optimization technique. The experimental data used for this purpose are listed in Table I. The Appendix describes the specific procedure used.

The optimized values of the five unknown input parameters are presented in Table III. The values of effective thermal conductivity and effective viscosity represent an enhancement of about two and 13 times, respectively, over the corresponding values for thermal conductivity and viscosity given in Table II. This behavior is consistent with the presence of turbulent flow in the weld pool during GTA welding, as reported in the literature.[5,32,34–36] De and DebRoy[5] reported the enhancement factors for thermal conductivity and viscosity in steel welds to be 4 and 15, respectively, using gradient-based optimization techniques. Hong *et al.*[34] suggested an enhancement factor between 12 and 15 for thermal conductivity and a factor more than 6 for the viscosity, while

TABLE III. Optimized values of the five unknown input parameters of the numerical heat transfer and fluid flow model.

Unknown variable	Value
Arc efficiency, η	0.72
Arc radius, r_b (mm)	2.8
Arc power distribution factor, d	0.21
Effective thermal conductivity of liquid metal, k_{eff}(J/m s K)	31.2
Effective viscosity of liquid metal, μ_{eff}(kg/m s)	0.061

using 150 A current and 25 V based on peak temperature analysis in the weld pool and $k-\varepsilon$ turbulence model calculations. Choo and Szekely[32] suggested an enhancement factor of 8 for thermal conductivity and a factor of 30 for the viscosity at a current of 100 A by matching the calculated weld pool geometry with the experimentally determined geometry. They also verified the weld pool shape and values of enhancement factors using the $k-\varepsilon$ turbulence model. Kumar and DebRoy[36] reported enhancement factors in the range of 5–9 for gas metal arc (GMA) fillet welding. The estimated values of arc efficiency, arc radius, and arc power distribution factor are 0.72, 2.8 mm, and 0.21, respectively, as shown in Table III. Choo et al.[37] have reported arc efficiency values higher than 0.68, while Mendez et al.[38] indicated the arc radius to be approximately 1.9 mm for currents of up to 300 A. The power distribution factor depends on the electrode angle and other experimental conditions and its value is often taken as 0.5. The differences in the values of the arc radius and the power distribution factor with their values reported in the literature are thought to be due to the differences in the experimental conditions. However, the values available in the literature[5,32,34–36] are specific to the welded material and welding conditions, and cannot be used for the welding of Ti–6Al–4V alloy. The optimized values of the unknown input parameters were used to calculate the weld geometry for the four sets of welding conditions listed in Table I. The calculated weld pool boundary is marked by the equilibrium solidus temperature of the Ti–6Al–4V alloy. Figures 1(a)–1(d) show good agreement between the calculated and the experimentally measured weld pool geometry indicating the appropriateness of the computed uncertain input parameters.

Figure 1 shows that for all the four welding conditions considered, the weld pool is wide and shallow because the Ti–6Al–4V alloy has a negative temperature coefficient of surface tension $(d\gamma/dT)$, which causes the liquid metal to move from the middle to the periphery on the surface of the weld pool. The relative importance of convection and conduction in the overall transport of heat in the weld pool can be assessed from the value of the Peclet number Pe, which is given by

$$Pe = \frac{u \rho C_P L}{k}, \tag{14}$$

where u is the velocity, ρ is the density, C_P is the specific heat at constant pressure, L is the characteristic length, and k is the thermal conductivity of the molten metal. When Pe is
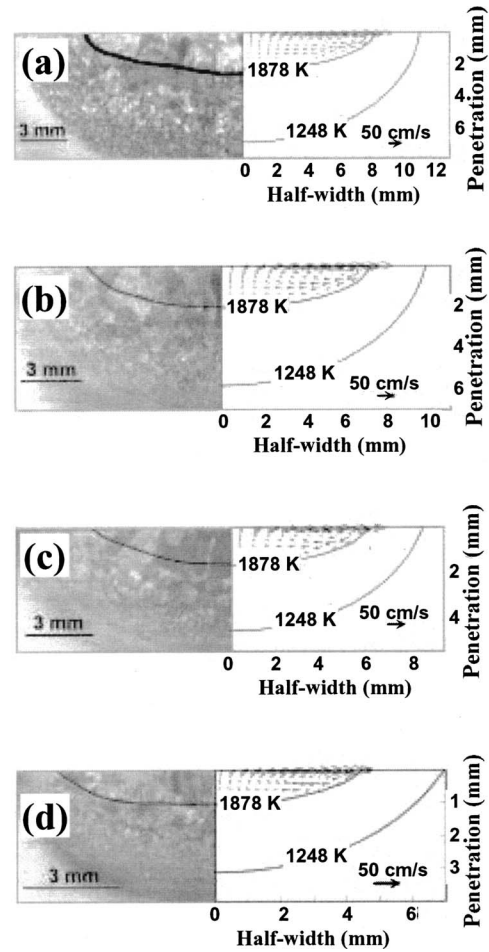
FIG. 1. Experimental weld geometry and the calculated weld geometry obtained using the optimum set of values of the unknown input parameters for the four sets of welding conditions given in Table I, i.e., (a) 111 A, 19.5 V, 0.5 mm/s; (b) 111.0 A, 19.2 V, 1.0 mm/s; (c) 111.0 A, 19.8 V, 2.0 mm/s; and (d) 111.0 A, 19.8 V, 4.0 mm/s. The length of the black arrow shows the magnitude of the velocities. In (b), (c), and (d) the four arrows on the experimental micro-graphs point at the fusion zone boundary. The 1878-K isotherm is the equilibrium solidus temperature of the Ti–6Al–4V alloy, which marks the fusion zone boundary. The outer isotherm is 1248 K, which is the β-transus temperature of the alloy(see. Ref. 7).

large, which in physical terms means large melt velocity, large weld pool, and poor thermal conductivity, heat is transported primarily by convection. For the weld pool shown in Fig. 1(c), the typical velocity in the pool is 0.11 m/s, density is 4000 kg/m³, specific heat is 700 J/kg K, characteristic length is 0.0061 m, and thermal conductivity[7] is 20 W/m K. The corresponding value of Pe is found to be 94, which is much larger than unity. This value of Pe indicates that heat is transported mainly by convection in the weld pool. Therefore, accurate calculations of the temperature field can only be done by considering convective heat transport. A fair agreement between the computed and the experimental weld dimensions indicates that the numerical heat transfer and fluid flow model, using the optimized values of the unknown input parameters, can provide both the expected trends and the correct weld geometry for various sets of welding conditions. After the values of the uncertain input parameters are determined, the calculation procedure can serve as a reliable link between the welding variables and the weld attributes such as the weld pool geometry.
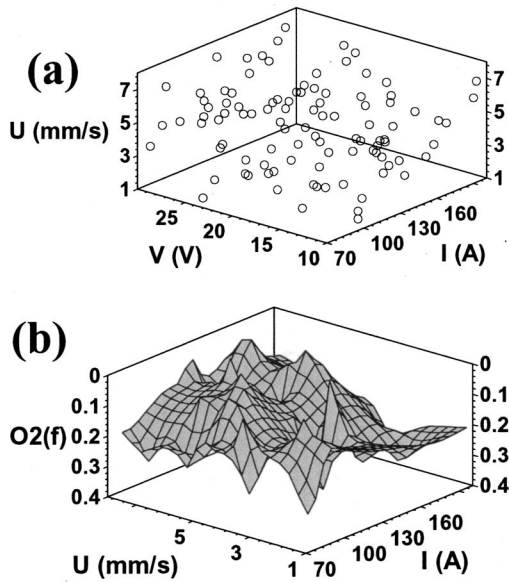
FIG. 2. Initial population of randomly chosen values of welding variable sets and their objective function values. (a) A large space of variables was searched to find optimum solutions as shown by the randomly selected initial welding variable sets. (b) The low values of the objective functions of several individuals in the initial population indicate the possibility of existence of multiple optimal solutions.

B. Calculating multiple sets of welding process variables

The calculation of the multiple sets of welding process variables to achieve a specified output or result from the proposed model involves three steps. First, a target weld geometry is identified by specifying the depth and width of the weld pool. Second, the proposed computational tool is utilized to calculate multiple sets of welding variables, i.e., various combinations of arc current, voltage, and welding speed, with each set capable of producing the same depth and width of the weld pool, i.e., the target weld geometry. Third and final, the results obtained from the model are adequately verified.

As a first step, the fourth set of experimental values of weld pool depth and width in Table I was chosen as the target weld geometry for the present study. Thus, one of the solutions determined by the proposed model must include the current, voltage, and welding speed combination used in the experiment considered. The other solutions calculated from the procedure must also be verified.

The second step, i.e., the calculation of the multiple sets of welding variables starts by specifying a large random population of potential solutions, i.e., randomly generated sets of values of welding variables of arc current, voltage, and welding speed. A population size of 100 welding variable sets was used. This number of variable sets was determined based on how the population size influenced the effectiveness of GA using standard test functions.[20,26,27] Figure 2(a) depicts the initial values of the individuals, i.e., sets of welding variables. Values of the variables were chosen within their appropriate ranges to maintain diversity of the variable values and explore a large domain of welding variables to include all possible solutions. These welding vari-
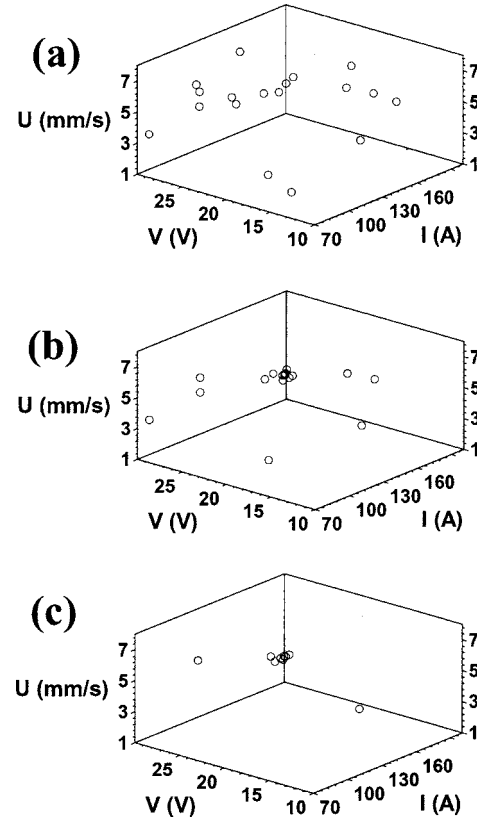
FIG. 3. Several fairly diverse welding variable sets could produce low values of the objective function indicating the existence of alternate paths to obtain the target weld geometry. The plots show the welding variable sets that produced low values of the objective function, O2(f) with iterations. (a) Individuals in the initial population with O2(f) less than 0.1; (b) individuals after five iterations with O2(f) less than 0.03; and (c) individuals after ten iterations with O2(f) less than 0.004.

able sets are then improved iteratively using a combination of GA and the reliable heat transfer and fluid flow model.

The progress of the iterations is monitored by calculating the objective function values, defined in Eq. (12), for each set of welding variables. An individual with a low objective function value indicates that the I, V, and U values it contains result in a small discrepancy between the computed and the target weld geometry. Figure 2(b) shows that for many sets of welding variables, the computed values of the objective function O2(f) are fairly low, indicating that each of these variable sets can produce a weld geometry that is close to the target geometry. Figures 3(a)–3(c) indicate several welding variable sets that have progressively lower objective function values. The objective functions are lower than 0.1, 0.03, and 0.004, corresponding to the first, fifth, and tenth generation of individuals, respectively. It is noteworthy that in Fig. 3, the sets of welding variables are distributed throughout the welding variable space, signifying the existence of multiple paths to attain the specified weld geometry. The progressive reduction of the objective function values of the best individuals indicates that the solutions are improved with iterations. When the values of the objective function are low and they do not decrease further with iterations, the computed welding variable sets constitute the final solutions, which are presented in Table IV.

TABLE IV. Optimized sets of values of welding variables, i.e., arc current (I), arc voltage (V), and welding speed (U), to achieve the following target weld pool dimensions: weld penetration =1.1 mm and weld width =9.6 mm. The target weld geometry was obtained experimentally using the following welding variables: I=111.0 A, V=19.8 V, and U=4.0 mm/s.

Individual solutions	Current (A)	Voltage (V)	Welding speed (mm/s)
(a)	115.2	19.7	4.4
(b)	183.3	15.5	6.5
(c)	144.4	19.0	6.2
(d)	126.2	21.5	5.9
(e)	145.6	14.5	3.4
(f)	98.7	26.6	6.0

Finally, the accuracy of each individual solution listed in Table IV was verified. The depth and width of the weld pool were calculated using the heat transfer and fluid flow model and the computed values were compared with those obtained experimentally. Note that the values of arc current, voltage, and welding speed in solution (a) of Table IV are almost the same as the corresponding experimental values listed in Table I. The solutions (b) to (f) exhibit significantly different values of the welding variables. The comparison between the computed and the experimental weld dimensions in Figs. 4(a)–4(f) show that all six sets of welding variables can lead to the same weld pool geometry. Furthermore, the same geometry was obtained using widely different values of the three welding parameters, indicating the diversity of the path through which the specified geometry can be obtained. For example, Table IV shows that the current values ranged from 99 to 183 A, voltages varied between 14.5 and 26.6 V, and the welding speed changed from 3.4 to 6.5 mm/s in various sets of optimized values. The fact that all these diverse viable paths can lead to the same weld pool dimensions clearly indicates the complexity and significant nonlinearity of the fusion welding system.
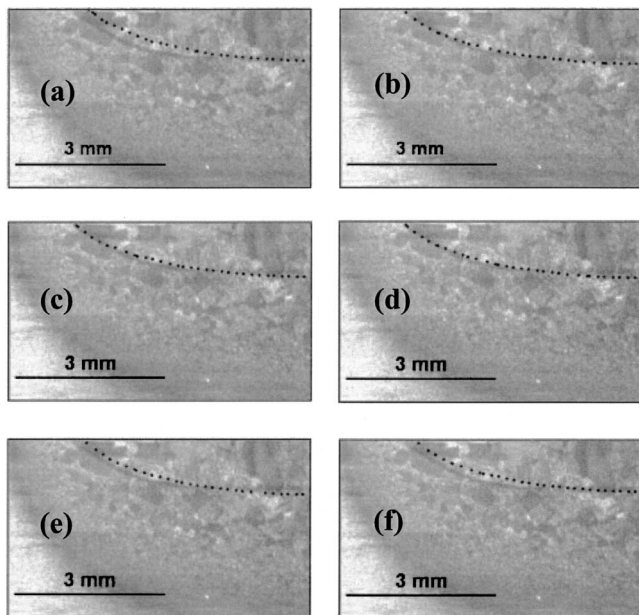
IV. SUMMARY AND CONCLUSIONS

The lack of reliability of the current thermofluid models of GTA welding in predicting fusion zone geometry and other parameters originates mainly from the uncertainty in the values of several input variables such as the arc efficiency, arc radius, arc power distribution factor, and effective thermal conductivity and viscosity of the molten metal. An engineering physics model for the calculation of heat transfer and fluid flow in fusion welding can be combined with an evolutionary optimization algorithm to enhance the reliability and utility of the computed temperature and velocity fields. By using a real-number-based GA, the values of these uncertain parameters were determined from a limited volume of experimental data for the GTA welding of Ti–6Al–4V alloy. The computed weld pool shape and size utilizing the optimized values of the uncertain parameters agreed well with the corresponding experimentally determined values for various welding conditions, indicating the effectiveness of the approach. The model was used to determine multiple sets of welding variables, i.e., combinations of welding current, voltage, and speed to obtain a specified weld pool geometry. It was found that a specific weld geometry was attainable via multiple pathways involving various sets of welding variables. Furthermore, these sets of welding variables involved significantly different values of current, voltage, and welding speed. Although the example presented here is concerned with restructuring of convective heat transfer models of fusion welding for tailoring weld geometry via multiple paths, it provides hope that other attributes of welds may also be tailored in the future using a combination of a thermofluid model and a GA.

FIG. 4. Comparisons between the calculated and the experimental weld pool geometry for different optimized combinations of welding variables given in Table IV. The calculated weld pool boundary is marked by a dotted line which represents the equilibrium solidus temperature of Ti–6Al–4V alloy at 1878 K.

APPENDIX: PARENT-CENTRIC- RECOMBINATION-(PCX) BASED GENERALIZED GENERATION GAP (G3) GENETIC ALGORITHM (GA)

The genetic algorithm used in the present study to calculate the optimized values of the unknown input parameters is a parent centric recombination (PCX) operator-based generalized generation gap (G3) model.[26,27] This model was chosen because it has been shown to have a faster convergence rate on standard test functions as compared to other evolutionary algorithms. The algorithm for the model is as follows:

(1) A population is a collection of many individuals and each individual represents a set of randomly chosen val-
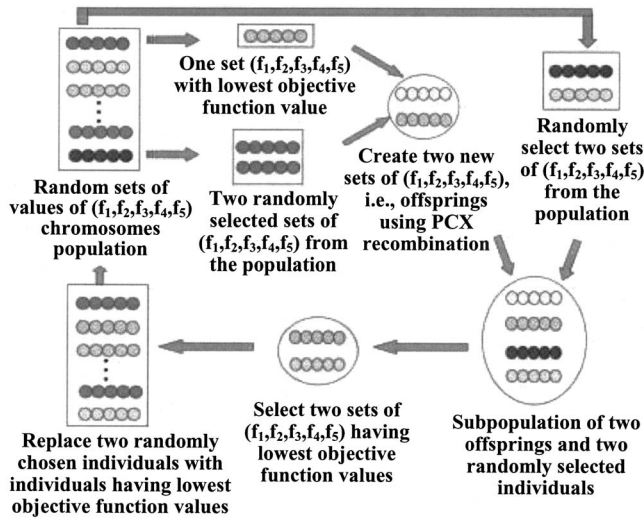
FIG. 5. Generalized generation gap (G3) model using parent centric recombination (PCX) operator.

FIG. 6. Flow chart of the G3 model.

ues of the five nondimensionalized unknown input parameters. A parent refers to an individual in the current population. The best parent is the individual that has the best fitness, i.e., gives the minimum value of the objective function, defined by Eq. (10), in the entire population. The best parent and two other randomly selected parents are chosen from the population.

(2) From the three chosen parents, two offsprings or new individuals are generated using a recombination scheme. PCX-based G3 models are known to converge rapidly when three parents and two offsprings are selected.[27] A recombination scheme is a process for creating new individuals from the parents.

(3) Two new parents are randomly chosen from the current population.

(4) A subpopulation of four individuals that includes the two randomly chosen parents in step (3) and two new offsprings generated in step (2) is formed.

(5) The two best solutions, i.e., the solutions having the least values of the objective function, are chosen from the subpopulation of four members created in step (4). These two individuals replace the two parents randomly chosen in step (3).

(6) The calculations are repeated from step (1) again until convergence is achieved.

The above steps, as applied to the present study, are shown in Fig. 5. The working of the model to find the unknown input variables by minimizing the objective function is illustrated in Fig. 6. The recombination scheme [step (2)] used in the present model is based on the PCX operator. A brief description of the PCX operator, as applied to the present problem of five unknown input parameters, is presented below.

First, three parents, i.e., $(f_1^0, f_2^0, f_3^0, f_4^0, f_5^0)$, $(f_1^1, f_2^1, f_3^1, f_4^1, f_5^1)$, and $(f_1^2, f_2^2, f_3^2, f_4^2, f_5^2)$, are randomly selected from the current population. Here, the subscripts represent the five unknown input parameters, while the superscripts denote the parent identification number. The mean vector or
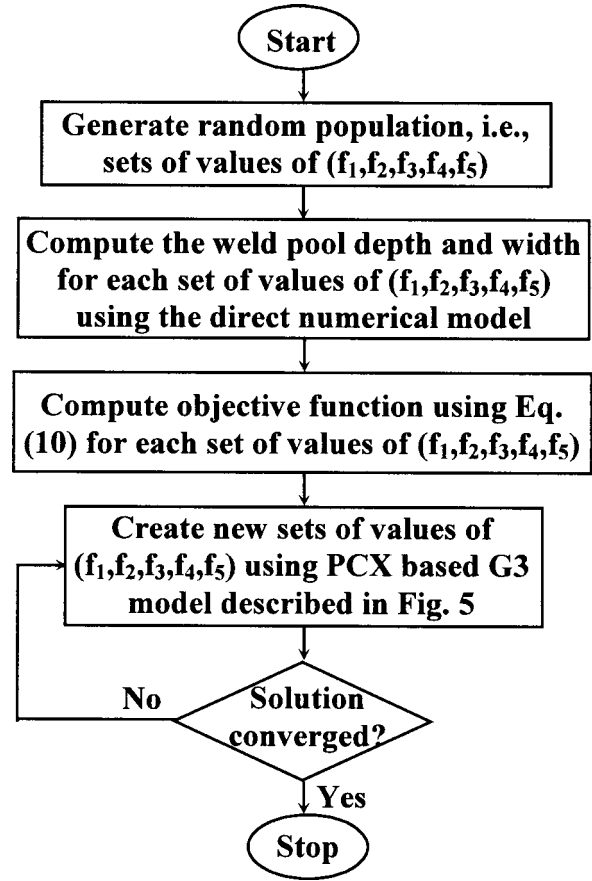
centroid, $\mathbf{g} = \left(\frac{f_1^0 + f_1^1 + f_1^2}{3}, \frac{f_2^0 + f_2^1 + f_2^2}{3}, \frac{f_3^0 + f_3^1 + f_3^2}{3}, \frac{f_4^0 + f_4^1 + f_4^2}{3}, \frac{f_5^0 + f_5^1 + f_5^2}{3} \right)$, of the three chosen parents is computed. To create an offspring, one of the parents, say $\mathbf{x}^{(p)} = (f_1^0, f_2^0, f_3^0, f_4^0, f_5^0)$ is chosen randomly. The direction vector, $\mathbf{d}^{(p)} = \mathbf{x}^{(p)} - \mathbf{g}$, is next calculated from the selected parent to the mean vector or centroid. Thereafter, from each of the other two parents, i.e., $(f_1^1, f_2^1, f_3^1, f_4^1, f_5^1)$ and $(f_1^2, f_2^2, f_3^2, f_4^2, f_5^2)$, perpendicular distances D_i to the direction vector $\mathbf{d}^{(p)}$ are computed and their average $\overline{D}$ is found. Finally, the offspring, i.e., $\mathbf{y} = (f_1', f_2', f_3', f_4', f_5')$, is created as follows:

$$\mathbf{y} = \mathbf{x}^{(p)} + w_\zeta |\mathbf{d}^{(p)}| + \sum_{i=1, i \neq p}^{5} w_\eta \overline{D} \mathbf{h}^{(i)}, \tag{A1}$$

where $\mathbf{h}^{(i)}$ are the orthonormal bases that span the subspace perpendicular to $\mathbf{d}^{(p)}$, and w_ζ and w_η are the randomly calculated zero-mean normally distributed variables. The values of the variables that characterize the offspring, $\mathbf{y} = (f_1', f_2', f_3', f_4', f_5')$, are calculated as follows:

$$f_1' = f_1^0 + f_{11} + f_{12}, \tag{A2a}$$

$$f_2' = f_2^0 + f_{21} + f_{22}, \tag{A2b}$$

$$f_3' = f_3^0 + f_{31} + f_{32}, \tag{A2c}$$

$$f_4' = f_4^0 + f_{41} + f_{42}, \tag{A2d}$$

$$f_5' = f_5^0 + f_{51} + f_{52}, \tag{A2e}$$

where

$$f_{11} = w_\zeta \left(\frac{2f_1^0 - f_1^1 - f_1^2}{3} \right), \tag{A3a}$$

$$f_{21} = w_\zeta \left(\frac{2f_2^0 - f_2^1 - f_2^2}{3} \right), \tag{A3b}$$

$$f_{31} = w_\zeta \left(\frac{2f_3^0 - f_3^1 - f_3^2}{3} \right), \tag{A3c}$$

$$f_{41} = w_\zeta \left(\frac{2f_4^0 - f_4^1 - f_4^2}{3} \right), \tag{A3d}$$

$$f_{51} = w_\zeta \left(\frac{2f_5^0 - f_5^1 - f_5^2}{3} \right), \tag{A3e}$$

$$f_{12} = w_\eta \left(\frac{a_2 + b_2}{2} \right) \left[1 - \left(\frac{2f_1^0 - f_1^1 - f_1^2}{3d} \right)^2 \right], \tag{A3f}$$

$$f_{22} = w_\eta \left(\frac{a_2 + b_2}{2} \right) \left[1 - \left(\frac{2f_2^0 - f_2^1 - f_2^2}{3d} \right)^2 \right], \tag{A3g}$$

$$f_{32} = w_\eta \left(\frac{a_2 + b_2}{2} \right) \left[1 - \left(\frac{2f_3^0 - f_3^1 - f_3^2}{3d} \right)^2 \right], \tag{A3h}$$

$$f_{42} = w_\eta \left(\frac{a_2 + b_2}{2} \right) \left[1 - \left(\frac{2f_4^0 - f_4^1 - f_4^2}{3d} \right)^2 \right], \tag{A3i}$$

$$f_{52} = w_\eta \left(\frac{a_2 + b_2}{2} \right) \left[1 - \left(\frac{2f_5^0 - f_5^1 - f_5^2}{3d} \right)^2 \right]. \tag{A3j}$$

The expressions for the variables d, a_2, and b_2, used in Eqs. (A3f)–(A3j), are as follows:

$$d = \sqrt{ \left(\frac{2f_1^0 - f_1^1 - f_1^2}{3} \right)^2 + \left(\frac{2f_2^0 - f_2^1 - f_2^2}{3} \right)^2 + \left(\frac{2f_3^0 - f_3^1 - f_3^2}{3} \right)^2 + \left(\frac{2f_4^0 - f_4^1 - f_4^2}{3} \right)^2 + \left(\frac{2f_5^0 - f_5^1 - f_5^2}{3} \right)^2 }, \tag{A4a}$$

$$a_2 = e_1 \times \sqrt{1 - (a_1)^2}, \tag{A4b}$$

$$b_2 = e_2 \times \sqrt{1 - (b_1)^2}, \tag{A4c}$$

$$a_1 = \sum_{i=1}^{5} \frac{(f_i^1 - f_i^0)((2f_i^0 - f_i^1 - f_i^2)/3)}{d \times e_1}, \tag{A4d}$$

$$e_1 = \sqrt{(f_1^1 - f_1^0)^2 + (f_2^1 - f_2^0)^2 + (f_3^1 - f_3^0)^2 + (f_4^1 - f_4^0)^2 + (f_5^1 - f_5^0)^2}, \tag{A4e}$$

$$b_1 = \sum_{i=1}^{5} \frac{(f_i^2 - f_i^0)((2f_i^0 - f_i^1 - f_i^2)/3)}{d \times e_2}, \tag{A4f}$$

$$e_2 = \sqrt{(f_1^2 - f_1^0)^2 + (f_2^2 - f_2^0)^2 + (f_3^2 - f_3^0)^2 + (f_4^2 - f_4^0)^2 + (f_5^2 - f_5^0)^2}. \tag{A4g}$$

[1]H. Zhao and T. DebRoy, J. Appl. Phys. **93**, 10089 (2003).

[2]W. Zhang, C.-H. Kim, and T. DebRoy, J. Appl. Phys. **95**, 5210 (2004).

[3]W. Zhang, C.-H. Kim, and T. DebRoy, J. Appl. Phys. **95**, 5220 (2004).

[4]A. De and T. DebRoy, J. Appl. Phys. **95**, 5230 (2004).

[5]A. De and T. DebRoy, J. Phys. D **37**, 140 (2004).

[6]S. Mishra and T. DebRoy, J. Phys. D **37**, 2191 (2004).

[7]S. Mishra and T. DebRoy, Acta Mater. **52**, 1183 (2004).

[8]X. He, P. Fuerschbach, and T. DebRoy, J. Appl. Phys. **94**, 6949 (2003).

[9]C.-H. Kim, W. Zhang, and T. DebRoy, J. Appl. Phys. **94**, 2667 (2003).

[10]A. Kumar and T. DebRoy, J. Appl. Phys. **94**, 1267 (2003).

[11]S. A. David, R. Trivedi, M. E. Eshelman, J. M. Vitek, S. S. Babu, T. Hong, and T. DebRoy, J. Appl. Phys. **93**, 4885 (2003).

[12]W. Zhang, G. G. Roy, J. W. Elmer, and T. DebRoy, J. Appl. Phys. **93**, 3022 (2003).

[13]X. He, P. Fuerschbach, and T. DebRoy, J. Phys. D **36**, 3079 (2003).

[14]X. He, P. W. Fuerschbach, and T. DebRoy, J. Appl. Phys. **96**, 4547 (2004).

[15]J. W. Elmer, T. A. Palmer, W. Zhang, B. Wood, and T. DebRoy, Acta Mater. **51**, 3333 (2003).

[16]T. Hong and T. DebRoy, Metall. Mater. Trans. B **34**, 267 (2003).

[17]K. Mundra, T. DebRoy, and K. Kelkar, Numer. Heat Transfer, Part A **29**, 115 (1996).

[18]A. Kumar, and T. DebRoy, Int. J. Heat Mass Transfer **47**, 5793 (2004).

[19]J. F. Lancaster, *The Physics of Welding*, 2nd ed.(Pergamon, Oxford, 1986).

[20]A. Kumar, S. Mishra, J. W. Elmer, and T. DebRoy, Metall. Mater. Trans. A **36**, 15 (2005).

[21]T. Hong, W. Pitscheneder, and T. DebRoy, Sci. Technol. Weld. Joining **3**, 33 (1998).

[22]T. Hong and T. DebRoy, Ironmaking Steelmaking **28**, 450 (2001).

[23]X. He, P. W. Fuerschbach, and T. DebRoy, J. Phys. D **36**, 1388 (2003).

[24]D. E. Goldberg, *Genetic Algorithm in Search, Optimization and Machine Learning* (Addison-Wesley, MA, 1989).

[25]*Handbook of Evolutionary Computations*, edited by T. Back, D. B. Fogel, and Z. Michalewicz (IOP, Bristol, 2000).

[26]K. Deb, A. Anand, and D. Joshi, Evol. Comput. **10**, 371 (2002).

[27]K. Deb, *Multi-objective Optimization Using Evolutionary Algorithms*, 1st ed.(Wiley, New York, 2001).

[28]V. R. Voller and C. Prakash, Int. J. Heat Mass Transfer **30**, 1709 (1987).

[29] A. D. Brent, V. R. Voller, and K. J. Reid, Numer. Heat Transfer **13**, 297 (1988).

[30] S. Kou and D. K. Sun, Metall. Trans. A **16**, 203 (1985).

[31] T. DebRoy, A. K. Mazumdar, and D. B. Spalding, Appl. Math. Model. **2**, 146 (1978).

[32] R. T. C. Choo and J. Szekely, Weld. J. (London) **73**, 25s (1994).

[33] Z. Yang and T. DebRoy, Metall. Mater. Trans. B **30**, 483 (1999).

[34] K. Hong, D. C. Weckmann, A. B. Strong, and W. Zheng, Sci. Technol. Weld. Joining **7**, 125 (2002).

[35] K. Hong, D. C. Weckmann, A. B. Strong, and W. Zheng, Sci. Technol. Weld. Joining **8**, 313 (2003).

[36] A. Kumar and T. DebRoy, J. Phys. D **38**, 127 (2005).

[37] R. T. C. Choo, J. Szekely, and R. C. Westhoff, Metall. Trans. B **23**, 357 (1992)

[38] P. F. Mendez, K. L. Niece, and T. W. Eagar, in *Proceedings from Materials Solutions Conference '99 on Joining of Advanced and Speciality Materials II*, edited by M. Singh, J. E. Indacochea, J. N. DuPont, K. Ikeuchi, and J. M. Fernandez (ASM International, Materials Park, OH 2000), pp. 151–158.